Power System Technology
ISSN:1000-3673

Received: 06-06-2024 Revised: 15-07-2024 Accepted: 28-08-2024

Numerical Investigation of a 3 kW Microturbine Combustion Chamber

Sinkevich M.V.[a], Borisov Y.A.[a], Khalife H. S.[b]

[a] Joint Institute of High Temperatures, Russian Academy of Sciences, 13 Bld. 2 Izhorskaya St, Moscow 125412, Russian Federation

[b] RUDN University, 6 Miklukho-Maklaya St, Moscow, 117198, Russian Federation

Abstract: Numerical simulation is crucial the development of microturbines because it allows to investigate the combustion process in the combustion chamber without the need of manufacturing expensive physical prototypes at early stages of development. This paper presents a numerical investigation of the combustion process occurring in a 3 kW microturbine combustion chamber. First, a computational model of an existing 30 kW microturbine combustion chamber design was developed. The results obtained were compared with experimental data to ensure the adequacy of the results obtained. After validation, a computational model of the 3 kW microturbine combustion chamber was developed. Three configurations of the 3 kW microturbine combustion chamber with different locations and numbers of dilution holes were investigated. Configuration 3 of the 3 kW microturbine combustion chamber showed the lowest standard deviation in outlet temperature (48.4 K) and velocity (29.7 m/s), indicating a more uniform temperature and velocity profile at the outlet compared to the other two configurations. While Configuration 3 had a higher pressure loss (1059 Pa) than the other configurations (939 and 836 Pa), the priority at this stage of development was placed on achieving optimal uniform temperature and velocity profiles at the combustion chamber outlet.

Keywords*: Microturbine, Combustion chamber, Numerical simulation.*

1. Introduction

Microturbines have emerged as efficient and compact power generation units for a wide range of applications, including distributed power generation, combined heat and power systems, and remote area electrification. These small gas turbines provide a reliable and flexible source of electricity, especially in areas with limited access to the traditional electrical grid. One of the key advantages of microturbines is their compact size and high portability, allowing for easier installation and transportation to different locations compared to larger gas turbine systems [1].

Microturbines typically consist of a compressor, combustion chamber, recuperator, turbine and generator combined into a compact unit. They can operate on a variety of fuels, including natural gas, propane, diesel and renewable fuels, providing fuel flexibility. The combustion chamber, which is a critical component of a microturbine, is pivotal in enabling the reliable functioning of the microturbine and the production of environmentally sustainable energy.

Power System Technology
ISSN:1000-3673
Received: 06-06-2024 Revised: 15-07-2024 Accepted: 28-08-2024

An efficient combustion chamber is necessary to minimize pollutant emissions and ensure stable and reliable operation of microturbines. Factors such as fuel and air mixing, residence time, flame stability and heat transfer, and uniform flow exiting the combustion chamber must be carefully considered during the design process. The combustion chamber of a microturbine must satisfy a wide range of requirements, the relative importance of which varies depending on the intended application. The main requirements are listed below:

1. High combustion efficiency (i.e. the fuel must burn completely so that all its chemical energy is released as heat);
2. Reliable and smooth ignition under various operating conditions;
3. Wide limits of stability (i.e. the flame must remain burning over a wide range of pressure and air/fuel ratio);
4. Minimal pressure loss;
5. Uniform outlet temperature and velocity profiles tailored to maximize turbine blade life;
6. Low emissions of smoke and gaseous pollutants;
7. Independence from pressure pulsations and other instabilities caused by combustion;
8. Size and shape compatible with microturbine casing;
9. Minimum cost and ease of manufacture;
10. Maintainability;
11. Durability;
12. Fuel flexibility.

Numerical simulation, particularly computational fluid dynamics (CFD), currently plays a significant role in studying and optimizing the combustion process in gas turbine combustion chambers. Several studies on the combustion chambers of gas turbines focus on exploring the use of alternative fuels like hydrogen and biofuels [2–8], as well as optimizing the chamber design and combustion parameters to improve efficiency and reduce emissions [9–18]. For instance, in the work [2], the different intrinsic components between natural gas and biogas and combustion performance of biogas in microturbine were studied. As the CO2 content in the biogas increased, the study found that nitrogen oxide (NO) and carbon monoxide (CO) emissions decreased, but the fuel flow rate and pressure drop within the combustion chamber had to be increased in order to maintain a constant thermal input. In the work [5] A CFD analysis of the reacting flow in a combustion chamber of a microturbine while using hydrogen – natural gas as a fuel. The study examined how the selection of different models for describing

Power System Technology
ISSN:1000-3673
Received: 06-06-2024 Revised: 15-07-2024 Accepted: 28-08-2024

the reacting flow within the combustor influenced the combustion process. Furthermore, in the work [16], the effects of various methane fuel blending ratios (0.19–0.41) on the combustion flow, emission characteristics, performance parameters, and field synergies were investigated through numerical simulation. Results obtained showed that the optimal fuel blending ratio for operating the SGT100 gas turbine is recommended to be in the range of 0.30 to 0.35. While in the work [18], the effects of varying the secondary oxygen ratio and fuel ratio on the flow field, temperature distribution, nitrogen oxide (NO) emissions, pressure loss, and field synergy within a micro gas turbine combustor were examined. Additionally, the sensitivity of two-stage combustion technologies on NO emissions was compared. The results showed that with the increase of secondary oxygen ratio from 0 % to 40 %, scope of central recirculation zone becomes smaller, outlet velocity grows, outlet temperature distribution factor becomes larger and pressure loss rises, the average outlet NO emission decreases from 20.2 ppm to 2.28 ppm, synergy angle of the central plane becomes larger, and the change mainly occurs in the recirculation zone and the rear of the combustion chamber.

The aim of this work is to numerically investigate different configurations of the 3 kW microturbine combustion chamber at an early stage of development of the microturbine. The CFD simulations will help identify an optimal design configuration by evaluating key performance criteria, with a focus on achieving uniform temperature and velocity profiles at the combustion chamber outlet.

2. Numerical simulation

2.1. Governing equations

ANSYS Fluent was used in this work to simulate the combustion process in microturbine combustor. Numerical simulations were performed using fundamental equations such as conservation of mass, momentum and energy, and the k-ε turbulence model equations.

The continuity equation describes the conservation of mass in a flow and is expressed as follows [19,20]:

$$\frac{\partial \rho}{\partial t} + \nabla \cdot (\rho \vec{u}) = S_m \tag{1}$$

where ∇ is gradient operator, ρ is the density, $\vec{u}$ is the velocity vector, and S_m is the source (mass added to the continuous phase from the dispersed second phase and any user-defined sources).

Conservation of momentum in an inertial (non-accelerating) reference frame is determined by the expression:

$$\frac{\partial}{\partial t}(\rho \vec{u}) + \nabla \cdot (\rho \vec{u}\vec{u}) = -\nabla p + \nabla \cdot (\bar{\bar{\tau}}) + \rho \vec{g} + \vec{F} \tag{2}$$

Power System Technology
ISSN:1000-3673
Received: 06-06-2024 Revised: 15-07-2024 Accepted: 28-08-2024

where P is the Static pressure, $\bar{\bar{\tau}}$ is the stress tensor, $\rho\vec{g}$ is the gravitational body force, and $\vec{F}$ are the external body forces.

The stress tensor is expressed by the formula:

$$\bar{\bar{\tau}} = \mu\left[\nabla\vec{u} + \vec{u}^T - \frac{2}{3}\nabla\cdot\vec{u}I\right] \tag{3}$$

where μ is the molecular viscosity, and I is the unit tensor.

Turbulent flows are characterized by complex vortex structures that cannot be accurately described by the Navier-Stokes equations. Therefore, various turbulence models are used to simulate turbulent flows [21,22]. The standard k-ε model is considered the most suitable model for simulating the combustion process in microturbine combustors with acceptable accuracy at an early stage of development of the microturbine.

The standard k-ε model is a semi-empirical model based on model transport equations for the kinetic energy of turbulence k and its dissipation rate ε. Transport equations for the standard k-ε model:

$$\frac{\partial}{\partial t}(\rho k) + \frac{\partial}{\partial x_i}(\rho k u_i) = \frac{\partial}{\partial x_j}\left[(\mu + \frac{\mu_t}{\sigma_k})\frac{\partial k}{\partial x_j}\right] + G_k + G_b - p\varepsilon - Y_m + S_k \tag{4}$$

$$\frac{\partial}{\partial t}(\rho\varepsilon) + \frac{\partial}{\partial x_i}(\rho\varepsilon u_i) = \\ = \frac{\partial}{\partial x_j}\left[(\mu + \frac{\mu_t}{\sigma_\varepsilon})\frac{\partial \varepsilon}{\partial x_j}\right] + C_{1\varepsilon}\frac{\varepsilon}{k}(G_k + C_{3\varepsilon}G_b) - C_{2\varepsilon}\rho\frac{\varepsilon^2}{k} + S_\varepsilon \tag{5}$$

where G_k is the generation of turbulence kinetic energy due to the mean velocity gradients, G_b is the generation of turbulence kinetic energy due to buoyancy, Y_m is the contribution of the fluctuating dilatation in compressible turbulence to the overall dissipation rate, $C_{1\varepsilon}, C_{2\varepsilon}, C_{3\varepsilon}$ are constants, $\sigma_k, \sigma_\varepsilon$ are the turbulent Prandtl numbers for k and ε, and S_k, S_ε are the user-defined source terms.

Turbulent (or eddy) viscosity μ_t is calculated by combining k and ε as follows:

$$\mu_t = \rho C_\mu \frac{k^2}{\varepsilon} \tag{6}$$

The model constants were chosen using default values in ANSYS Fluent and are the most widely used [22].

Conservation of energy is given by [23]:

Power System Technology
ISSN:1000-3673
Received: 06-06-2024 Revised: 15-07-2024 Accepted: 28-08-2024

$$\frac{\partial}{\partial t}(\rho E) + \nabla \cdot \left(\vec{u}(\rho E + p)\right) = \nabla \cdot (\lambda_{eff} \nabla T - \sum_j h_j \vec{j}_j + (\bar{\bar{\tau}}_{eff} \cdot \vec{u})) + S_h \quad (7)$$

where λ_{eff} is the effective thermal conductivity, which includes the turbulent thermal conductivity determined by the selected turbulent model, $\vec{j}_j$ is the diffusion flux of species j, and S_h is the heat of chemical reaction, and any other volumetric heat sources defined by user.

The fuel and oxidizer combustion characteristics were determined using the non-premixed combustion model. This combustion model assumes a probability density function (PDF) to calculate the chemical turbulence mechanism.

The basis of the non-premixed combustion model is that, under a certain set of simplifying assumptions, the instantaneous thermochemical state of the liquid is related to a conserved scalar quantity known as the mixture fraction f. The mixture fraction can be written in terms of the atomic mass fraction as [24]:

$$f = \frac{Z_i - Z_{i,ox}}{Z_{i,fuel} - Z_{i,ox}} \quad (8)$$

where Z_i is the elemental mass fraction for element *i*. The subscript ox denotes the inlet value of the oxidizer stream, and the subscript fuel denotes the value at the inlet of the fuel stream.

2.2. Computational model and boundary conditions

First, a computational model of an existing design of a 30 kW microturbine combustion chamber was developed as shown in **Fig. 1.**

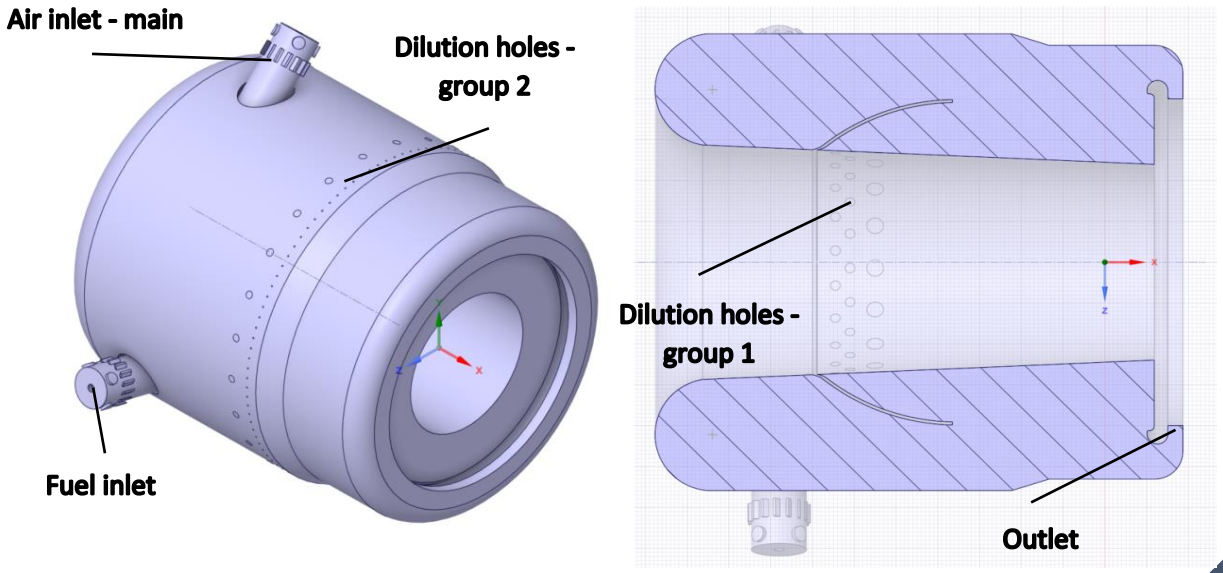

Fig. 1 Model of the 30 kW microturbine combustion chamber

Power System Technology
ISSN:1000-3673
Received: 06-06-2024 Revised: 15-07-2024 Accepted: 28-08-2024

Calculations were carried out using boundary conditions based on the nominal operation of the 30 kW microturbine using methane as fuel. The boundary conditions of the model are given in **Table 1**.

Table 1: Boundary conditions of the 30 kW microturbine combustion chamber model

Parameter	Nominal value
Air inlet pressure, kPa	354
Air inlet temperature, K	812
Fuel inlet temperature, K	300
Fuel mass flow rate, kg/s	0.0024
Type of fuel	Methane (CH4)
Gas mass flow rate at the outlet, kg/s	0.31

To validate the model of the 30 kW microturbine combustion chamber, experimental data were used. The average temperature at the combustion chamber outlet and pressure loss were chosen as the key parameters for validation of the developed computational model. The validation process is highly important and serves as the basis for the subsequent development and simulation of the 3 kW microturbine combustion chamber model, which is considered a more compact design of the 30 kW microturbine combustion chamber.

The design of the 3 kW microturbine combustion chamber takes into account the main features of the 30 kW microturbine combustion chamber, such as the radial arrangement of the injectors, the flow divider inside the chamber and the location of the dilution holes (**Fig. 2**). The dilution holes on both sides of the combustion chamber were also divided into two groups. It is also worth noting that the stator section is included in the model as seen in **Fig. 2**. This is done to ensure adequate results of the calculations based on the chosen boundary conditions; however, all outlet parameters were evaluated before the stator section.

Power System Technology
ISSN:1000-3673
Received: 06-06-2024 Revised: 15-07-2024 Accepted: 28-08-2024

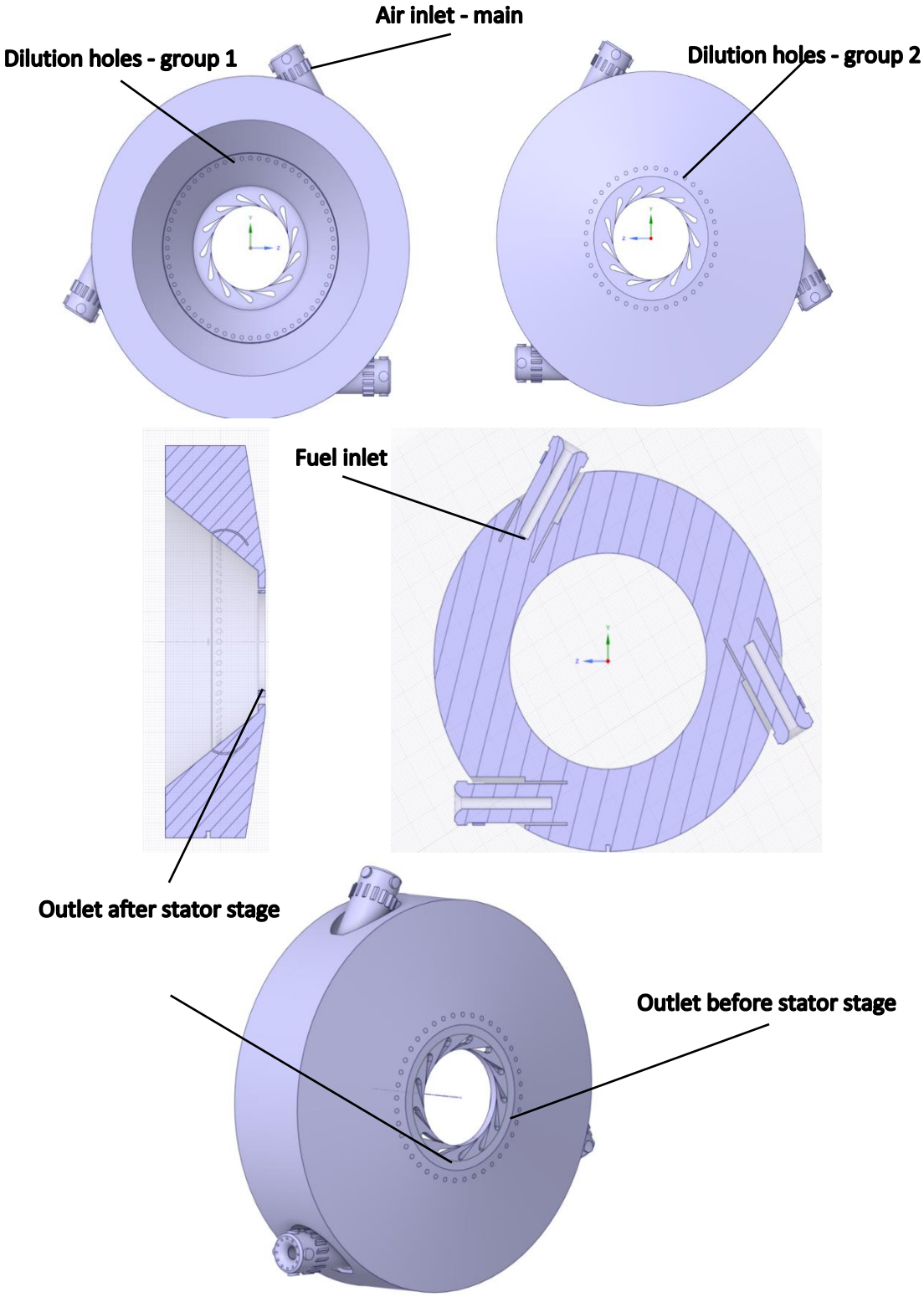

Fig. 2 Model of the 3 kW microturbine combustion chamber

Power System Technology
ISSN:1000-3673
Received: 06-06-2024 Revised: 15-07-2024 Accepted: 28-08-2024

Calculations were also carried out using boundary conditions based on the calculated parameters of nominal operation of the 3 kW microturbine using methane as fuel. The boundary conditions of the model are given in **Table 2**.

Table 2: Boundary conditions of the 3 kW microturbine combustion chamber model

Parameter	Nominal value
Air inlet pressure, kPa	248
Air inlet temperature, K	943
Fuel inlet temperature, K	300
Fuel mass flow rate, kg/s	0.000394
Type of fuel	Methane (CH4)
Gas mass flow rate at the outlet, kg/s	0.059

In order to investigate the operation of the combustion chamber and optimize the flow characteristics, three configurations with different locations and numbers of dilution holes were studied, as shown in **Fig. 3**.

Configuration 1	Configuration 2	Configuration 3
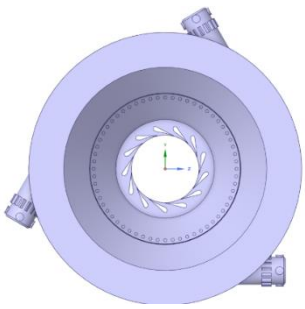	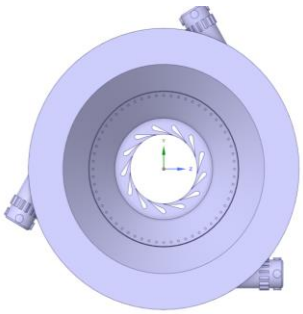	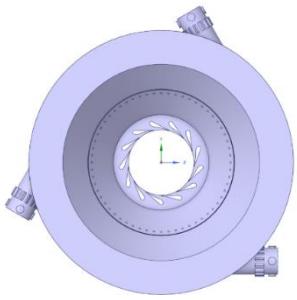
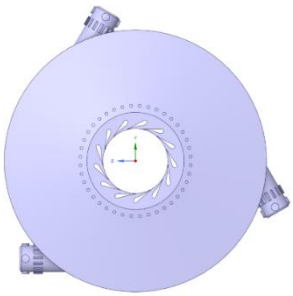	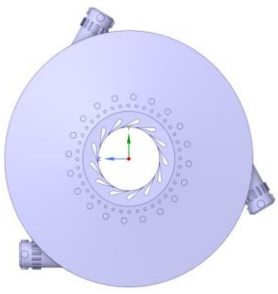	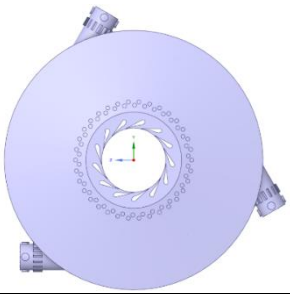

Fig. 3 Configurations of the 3 kW microturbine combustion chamber with different locations and numbers of dilution holes.

Power System Technology
ISSN:1000-3673
Received: 06-06-2024 Revised: 15-07-2024 Accepted: 28-08-2024

The primary function of the dilution zone is to provide an outlet stream with a uniform temperature distribution that is suitable for the downstream turbine [1]. Uniform temperature and velocity profiles at the outlet of the combustion chamber were considered the main parameters to choose an optimal configuration in this work. While pressure loss was also considered in choosing the optimal configuration, it was given a lower priority compared to the importance of achieving uniform temperature and velocity profiles at the combustion chamber outlet. The main design parameters of the dilution holes in the three configurations are given in **Table 3**.

Table 3: Design parameters of the dilution holes in the 3 kW microturbine combustion chamber

	Configuration 1	Configuration 2	Configuration 3
First group			
Number of holes	60	60	60
Diameter, mm	3	2	2
	Second group		
Number of holes	40	20/40	68
Diameter, mm	3	6/3	4

2.3. Mesh independence test

To determine the minimum number of elements required to obtain accurate results with minimal computational resources, meshes of different densities were created. Combustion chamber models with different mesh densities were simulated under the same boundary conditions.

Three models were developed with different mesh densities: 1.7, 1 and 0.8 million elements for the model of the 30 kW microturbine combustion chamber. The temperature profiles along a selected line for the three different meshes developed are shown in **Fig. 4**. From the results, it can be seen that a model with 1 million elements is sufficient to provide acceptable results, since further increasing the number of elements leads to insignificant changes in the results. In addition, the average outlet temperature for all three models showed the same results (≈1130 K). Therefore, the mesh of 1 million elements was used to simulate the combustion processes occurring in the 30 kW microturbine combustion chamber.

Power System Technology
ISSN:1000-3673
Received: 06-06-2024 Revised: 15-07-2024 Accepted: 28-08-2024

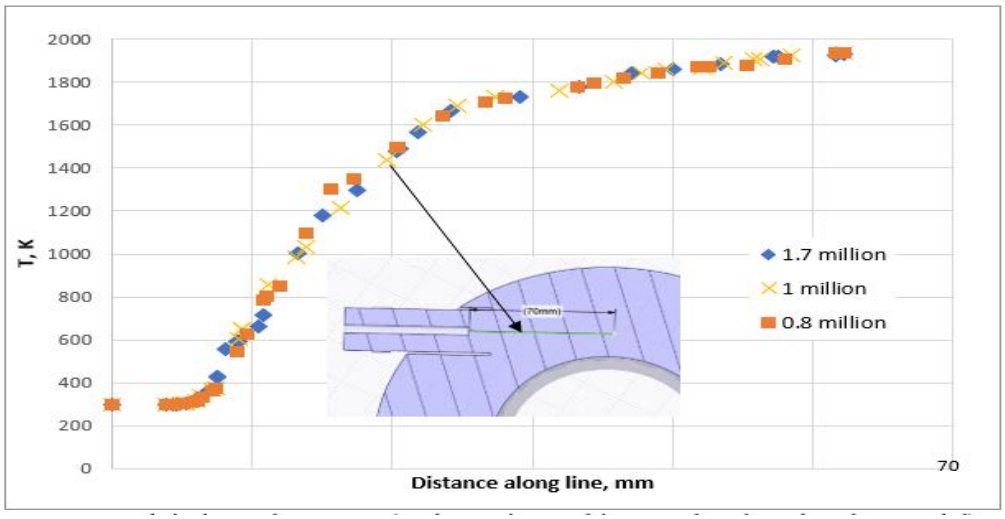

Fig. 4 Mesh independence test (30 kW microturbine combustion chamber model).

For the 3 kW microturbine combustion chamber model, three models with different mesh densities were also developed: 2.7, 1.3 and 0.8 million elements. The temperature profiles along the selected line for the three different meshes developed are shown in **Fig. 5**. From the results, it can be seen that the model with 1.3 million elements is sufficient to provide acceptable results, since further increases in the number of elements lead to minor changes in the results. In addition, the average outlet temperature for all three models showed the same results (≈1209 K). Therefore, the mesh of 1.3 million elements was used to simulate the combustion processes occurring in the 3 kW microturbine combustion chamber.

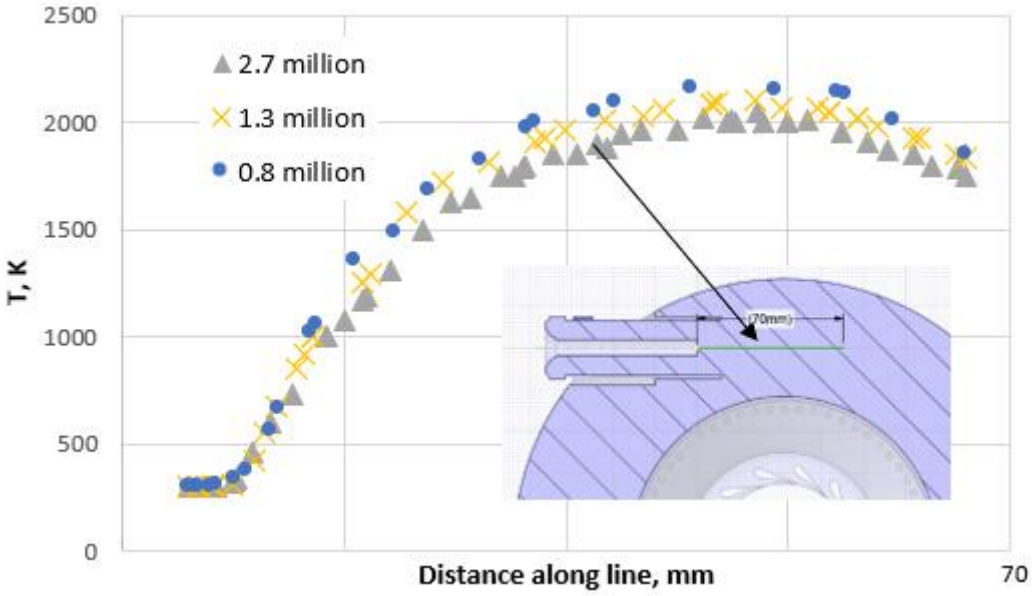

Fig. 5 Mesh independence test (3 kW microturbine combustion chamber model).

Power System Technology
ISSN:1000-3673
Received: 06-06-2024 Revised: 15-07-2024 Accepted: 28-08-2024

3. Results

3.1. Validation of the 30 kW microturbine combustion chamber model

To validate the 30 kW microturbine combustion chamber, experimental data of the outlet temperature and pressure loss were used. The mass-weighted average temperature of the gas at the outlet of the combustion chamber, obtained as a result of calculations, was 1130 K as shown in **Fig. 6**. The measured outlet temperature of the exhaust gas at the outlet from the combustion chamber was 1113-1128 K. The deviation from the measured temperature was 1.5-0.2%. Furthermore, the pressure loss in the combustion chamber, obtained as a result of calculations, was 4653 Pa. The measured pressure loss in the combustion chamber was 4829-5230. The deviation from the measured pressure loss was 3.6-11%.

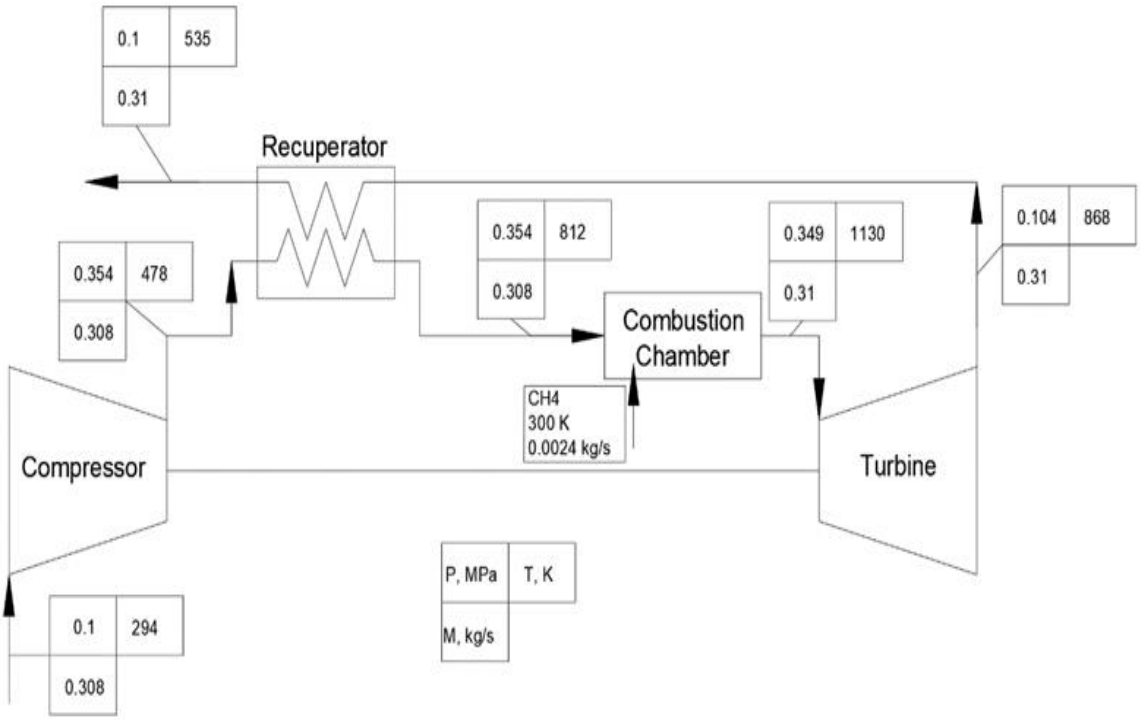

Fig. 6 Schematic diagram of the 30 kW microturbine

Temperature distribution inside the 30 kW microturbine combustion chamber is shown in **Fig. 7.** The results show good mixing in the combustion zone at the outlet of the injectors, then the combustion products are cooled down by flow exiting the dilution holes, leading to a uniform temperature profile at the outlet of the chamber. The standard deviation of temperature at the outlet was about 73 K.

Power System Technology
ISSN:1000-3673
Received: 06-06-2024 Revised: 15-07-2024 Accepted: 28-08-2024

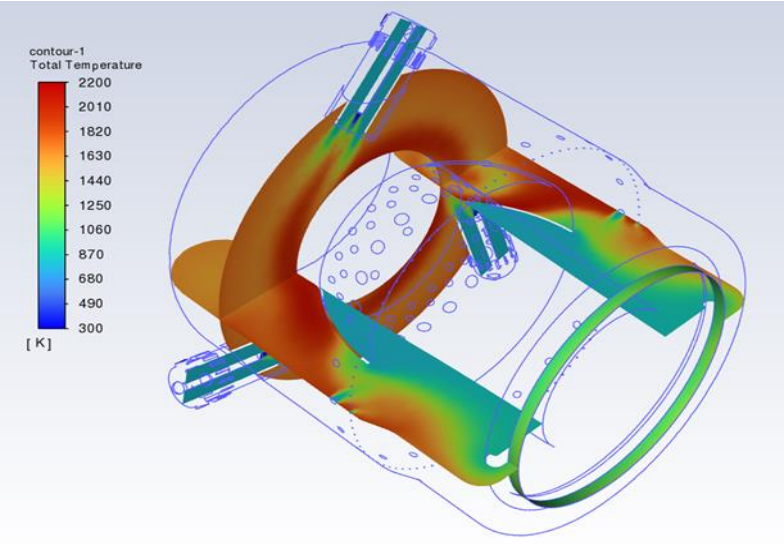

Fig. 7 Temperature distribution inside the 30 kW microturbine combustion chamber

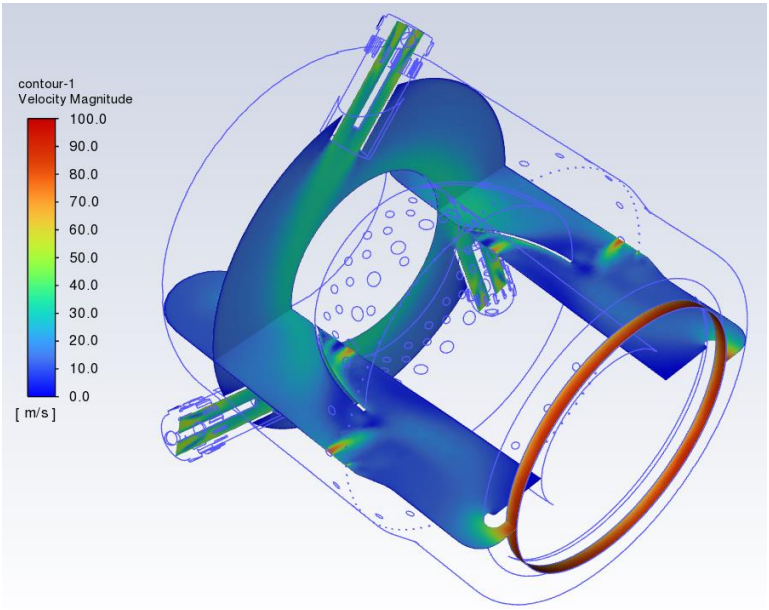

Fig. 8 Velocity distribution inside the 30 kW microturbine combustion chamber

In addition, velocity distribution inside the 30 kW microturbine combustion chamber is shown in **Fig. 8.** The results show the locations of high velocity flow exiting the dilution holes which lead to a good mixing in the combustion chamber. A uniform velocity profile was also achieved at the outlet of the combustion chamber. The standard deviation of velocity at the outlet was about 12 m/s.

Achieving uniform temperature and velocity profiles at the outlet of the combustion chamber confirms the suitable locations and number of dilution holes. After validation of the developed

Power System Technology
ISSN:1000-3673
Received: 06-06-2024 Revised: 15-07-2024 Accepted: 28-08-2024

model of the 30 kW microturbine combustion chamber, calculations were conducted on three different configurations of the 3 kW microturbine combustion chamber in order to identify an optimal design at the current stage of development of the 3 kW microturbine.

3.2. Comparison of three 3 kW microturbine combustion chamber configurations

The results of calculations performed on the three configurations of the 3 kW microturbine combustion chamber are presented in **Table 4**. The lowest standard deviation of the outlet temperature (48.4 K) and velocity (29.7 m/s) were obtained in Configuration 3, which suggests a more uniform temperature and velocity at the outlet compared to the first two configurations. While the pressure loss in configuration 3 (1059 Pa) was higher than the other two configurations (939 and 836 Pa), the difference was not significant. At this stage of the 3 kW microturbine's development, the priority was placed on achieving the optimal uniform temperature and velocity profiles at the combustion chamber outlet, rather than minimizing the pressure loss.

Table 4: Calculation results of the 3 kW microturbine combustion chamber

Parameter	Configuration 1	Configuration 2	Configuration 3
Pressure loss, Pa	939	836	1059
Average velocity at outlet, m/s	78.8	79.5	79.3
Average temperature at outlet, K	1207.4	1210.2	1211.3
Standard deviation at outlet (Velocity), m/s	30.6	30.1	29.7
Standard deviation at outlet (Temperature), K	189.1	83.6	48.4

The temperature profile at outlet of the combustion chamber for the three configurations is shown in **Fig. 9.** It can be seen that the most uniform temperature profile at the outlet of the combustion chamber was achieved in configuration 3. Maintaining a constant temperature profile at the outlet of the combustion chamber is important for the turbine, since it ensures optimal efficiency, protects the turbine blades from thermal damage, reduces mechanical stress on the turbine components and allows for better control and prediction of the turbine operation.

Power System Technology
ISSN:1000-3673
Received: 06-06-2024 Revised: 15-07-2024 Accepted: 28-08-2024

Configuration 1 Configuration 2 Configuration 3

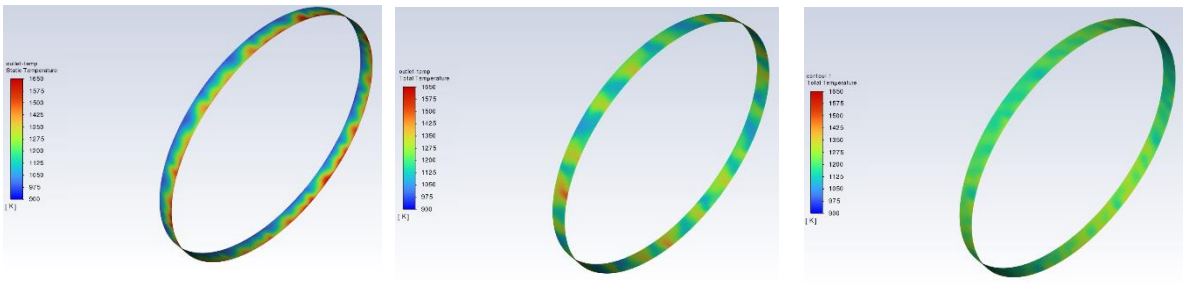

Fig. 9 Temperature profile at outlet of the 3 kW microturbine combustion chamber

The velocity profile at outlet of the combustion chamber for the three configurations is shown in **Fig. 10.** The exit velocity for all three configurations is almost the same (≈79 m/s), which is expected since the boundary conditions were the same. Among the three configurations evaluated, configuration 3 exhibited a slightly better velocity profile, as indicated by a lower standard deviation of the outlet velocity (29.7 m/s) compared to the other two configurations (30.6 and 30.1 m/s).

The segmental nature of the velocity profile shown in **Fig. 10** is attributed to the presence of the stator section downstream of the combustion chamber (**Fig. 2**). The stator section was included to ensure adequate results of the calculations based on the boundary conditions chosen. The uniform velocity profile helps improve the aerodynamic performance of the turbine blades, reducing the risk of flow separation and increasing overall efficiency. It also helps minimize mechanical stress on the turbine components, preventing uneven loading and potential structural damage.

Configuration 1 Configuration 2 Configuration 3

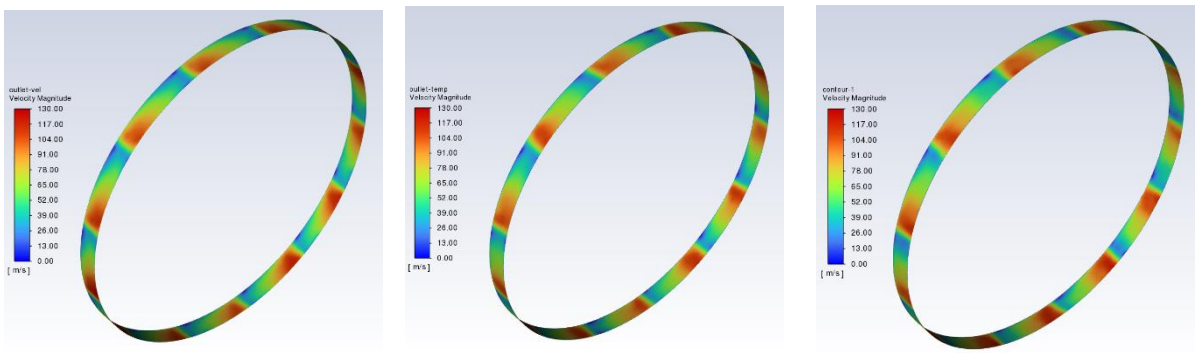

Fig. 10 Velocity profile at outlet of the 3 kW microturbine combustion chamber

Power System Technology
ISSN:1000-3673
Received: 06-06-2024 Revised: 15-07-2024 Accepted: 28-08-2024

The temperature and velocity distribution in the primary zone of the combustion chamber is shown in **Fig. 11 and Fig.12.** In all three configurations, methane burns in the primary zone of the combustion chamber after exiting the injector, indicating good air-fuel mixing. However, the difference in the location and size of dilution holes had an effect on the combustion efficiency due to change of air mass flow through the injectors (**Fig. 13)**. More air flowing through the injectors in configuration 1 (0.020 kg/s) compared to the other configurations (0.017 and 0.019 kg/s) lead to a better combustion in the primary zone and justifies the higher temperature in the cross-section shown in **Fig. 11.**

Configuration 1 Configuration 2 Configuration 3

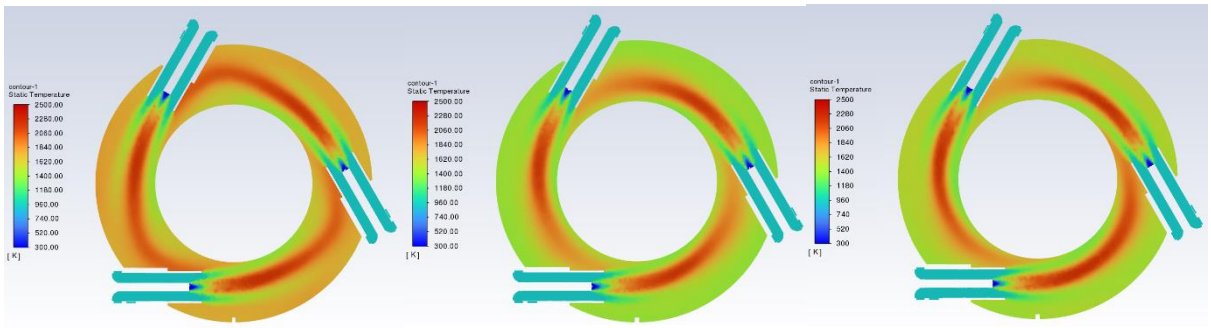

Fig. 11 Temperature distribution in the cross-section X= -49 mm of the 3 kW microturbine combustion chamber

Configuration 1 Configuration 2 Configuration 3

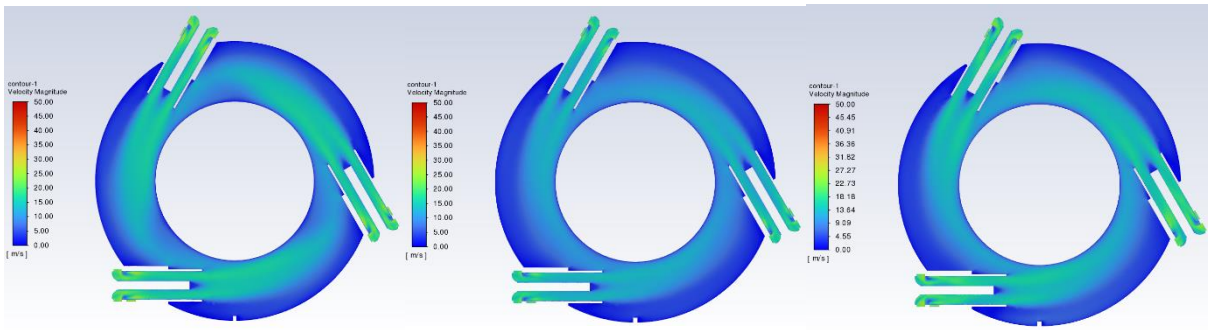

Fig. 12 Velocity distribution in the cross-section X= -49 mm of the 3 kW microturbine combustion chamber

Power System Technology
ISSN:1000-3673
Received: 06-06-2024 Revised: 15-07-2024 Accepted: 28-08-2024

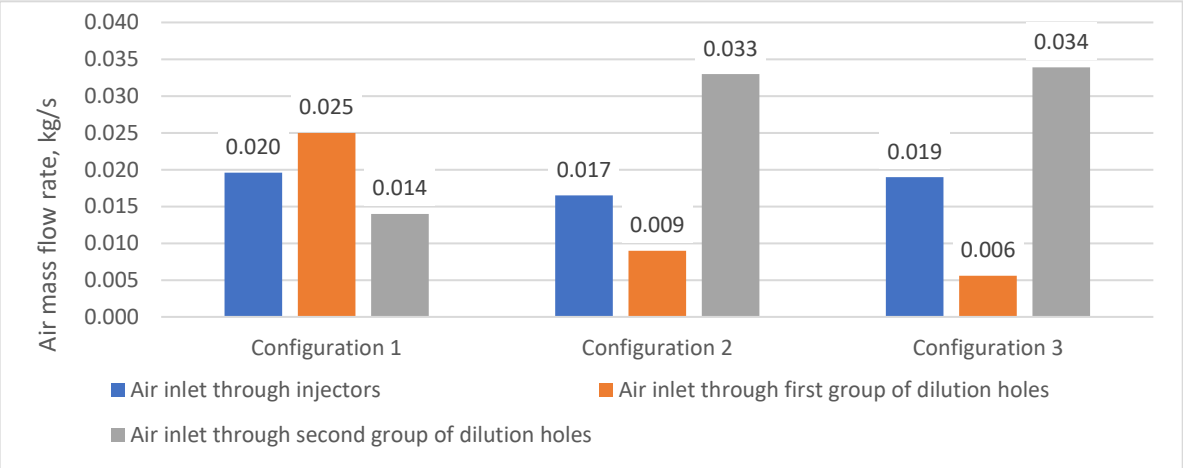

Fig. 13 Air mass flow rate at the inlet of the 3 kW microturbine combustion chamber

Another important effect of altering the location and size of the dilution hole groups can be seen in the gas temperature at the exit of the combustion chamber and in another cross-section of the chamber, as shown in **Fig.14** and **Fig. 15**.

Analyzing **Fig.14** and **Fig. 15**, it is evident that the increased air mass flow through the second group of dilution holes while maintaining a high air mass flow through the injectors in Configuration 3 had the major impact on providing a uniform temperature and velocity profiles at the outlet of the combustion chamber with minimal deviations compared to the other two configurations.

The first group of dilution holes in the 3 kW microturbine combustion chamber had a minimal effect on the temperature and velocity at the outlet due to the narrow channel after the flow divider, and the small distance to the outlet as shown in **Fig.14** and **Fig. 15.** Unlike the case in the 30 kW microturbine combustion chamber, the distance to the outlet and the diameter of the channel after the flow divider are larger (**Fig. 1**), which allows the mixing the combustion products with cold air even before exiting the chamber.

Configuration 1 Configuration 2 Configuration 3

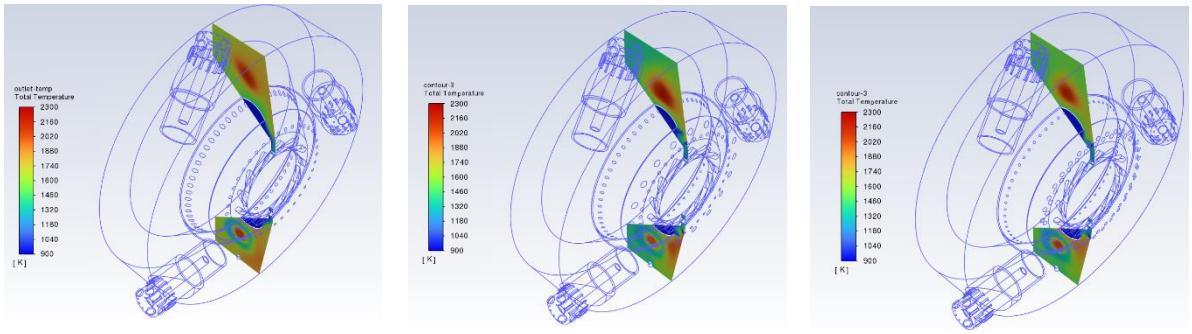

Power System Technology
ISSN:1000-3673
Received: 06-06-2024 Revised: 15-07-2024 Accepted: 28-08-2024

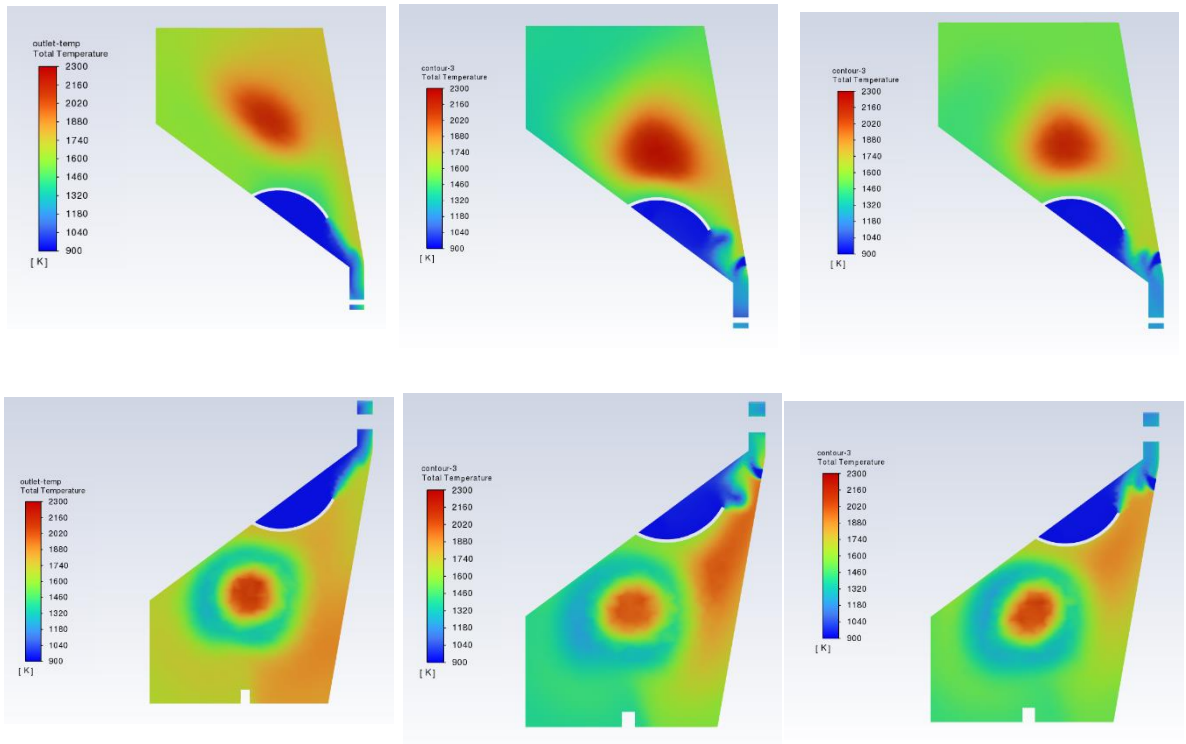

Fig. 14 Temperature profile in the cross-section Z= 0 mm of the 3 kW microturbine combustion chamber

Configuration 1 Configuration 2 Configuration 3

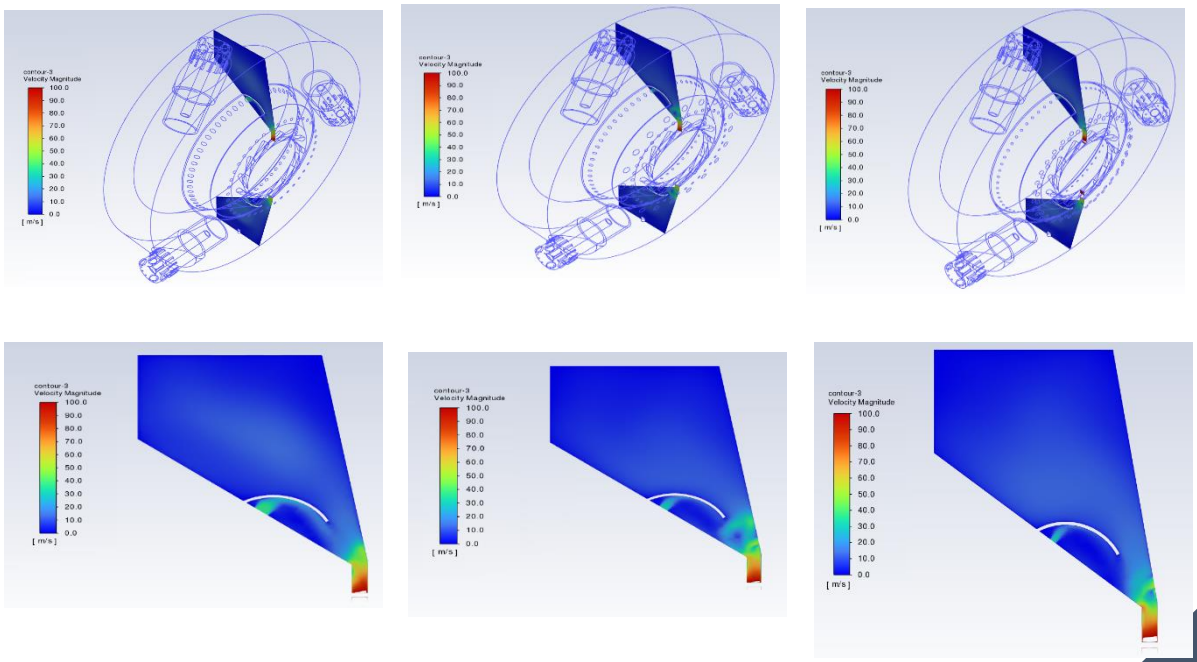

Power System Technology
ISSN:1000-3673
Received: 06-06-2024 Revised: 15-07-2024 Accepted: 28-08-2024

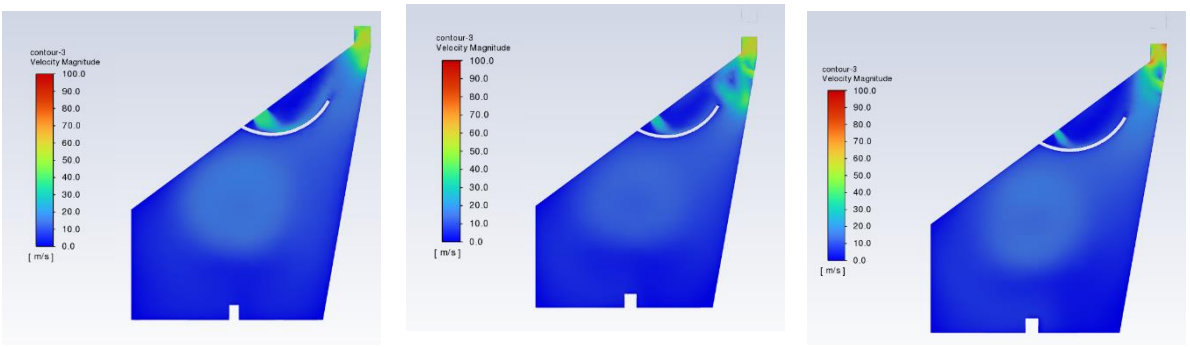

Fig. 15 Velocity profile in the cross-section Z= 0 mm of the 3 kW microturbine combustion chamber

4. Conclusion

This paper presents a numerical investigation of the combustion process in a 3 kW microturbine combustion chamber. A computational model of an existing 30 kW microturbine combustion chamber was first developed and validated against experimental data. After that a model of a 3 kW microturbine combustion chamber was developed. The design of the 3 kW microturbine combustion chamber took into account the main features of the 30 kW microturbine combustion chamber, such as the radial arrangement of the injectors, the flow divider inside the chamber and the location of the dilution holes. Three configurations of the 3 kW microturbine combustion chamber with different locations and numbers of dilution holes were investigated to achieve optimal flow through the combustion chamber and uniform temperature and velocity profiles at the outlet of the combustion chamber. The main conclusions of this paper can be summarized as follows:

1. The computational model of the 30 kW microturbine combustion chamber was validated against experimental data, showing good agreement in outlet temperature (deviation of 0.2-1.5%) and pressure loss (deviation of 3.6-11%).
2. Configuration 3 of the 3 kW microturbine combustion chamber showed the lowest standard deviation in outlet temperature (48.4 K) and velocity (29.7 m/s), indicating a more uniform temperature and velocity profile at the outlet compared to the other two configurations.
3. While Configuration 3 had a higher pressure loss (1059 Pa) than the other configurations (939 and 836 Pa), the priority at this stage of development was placed on achieving optimal uniform temperature and velocity profiles at the combustion chamber outlet.
4. The increased air mass flow through the second group of dilution holes in configuration 3, while maintaining a high air mass flow through the injectors, was the key factor in

Power System Technology
ISSN:1000-3673
Received: 06-06-2024 Revised: 15-07-2024 Accepted: 28-08-2024

providing the most uniform temperature and velocity profiles at the combustion chamber outlet.

5. The first group of dilution holes had a minimal effect on the temperature and velocity at the outlet due to the narrow channel and small distance to the outlet, unlike the case of the 30 kW microturbine where the larger distance and diameter allowed for better mixing of the combustion products with cold air even before exiting the chamber.

In future work, the main focus will be on changing the size of the injectors in order to determine the effect on air and fuel mixing in the primary zone of the combustion chamber and the uniformity of the flow at the outlet. Additionally, the effect of the flow on the combustion chamber wall temperature will be investigated to ensure the structural integrity of the system.

Refrences

[1] Lefebvre Arthur H., Ballal Dilip R., Gas Turbine Combustion Alternative Fuels and Emissions, 3rd ed., CRC Press Taylor & Francis Group, 6000 Broken Sound Parkway NW, Suite 300, 2010.

[2] X. Chen, W. Zhou, Y. Jia, J. Tang, Numerical Analysis of the Combustion in Micro Gas Turbine with Methane/Biogas Fuels, Arab J Sci Eng 46 (2021) 11897–11907. https://doi.org/10.1007/s13369-021-05731-3.

[3] S. Serbin, K. Burunsuz, D. Chen, J. Kowalski, Investigation of the Characteristics of a Low-Emission Gas Turbine Combustion Chamber Operating on a Mixture of Natural Gas and Hydrogen, Polish Maritime Research 29 (2022) 64–76. https://doi.org/10.2478/pomr-2022-0018.

[4] S. Tamang, H. Park, Numerical investigation of combustion characteristics for hydrogen mixed fuel in a can-type model of the gas turbine combustor, Int J Hydrogen Energy 48 (2023) 11493–11512. https://doi.org/10.1016/j.ijhydene.2022.05.273.

[5] R. De Robbio, Innovative combustion analysis of a micro-gas turbine burner supplied with hydrogen-natural gas mixtures, in: Energy Procedia, Elsevier Ltd, 2017: pp. 858–866. https://doi.org/10.1016/j.egypro.2017.08.291.

[6] K. Wang, F. Li, T. Zhou, Y. Ao, Numerical Study of Combustion and Emission Characteristics for Hydrogen Mixed Fuel in the Methane-Fueled Gas Turbine Combustor, Aerospace 10 (2023). https://doi.org/10.3390/aerospace10010072.

[7] S. Cordiner, V. Mulone, Experimental-numerical analysis of a biomass fueled microgeneration power-plant based on microturbine, Appl Therm Eng 71 (2014) 905–912. https://doi.org/10.1016/j.applthermaleng.2014.02.015.

[8] W. Pan, L. Kang, Z. Chi, W. Wang, C. Tang, Numerical study on effects of hydrogen doping of natural gas on the combustion characteristics in micro gas turbine combustor,

Power System Technology
ISSN:1000-3673
Received: 06-06-2024 Revised: 15-07-2024 Accepted: 28-08-2024

Appl Therm Eng (2024) 123989. https://doi.org/10.1016/J.APPLTHERMALENG.2024.123989.

[9] S. Serbin, K. Burunsuz, Numerical study of the parameters of a gas turbine combustion chamber with steam injection operating on distillate fuel, International Journal of Turbo & Jet-Engines 40 (2023) 71–80. https://doi.org/10.1515/tjj-2020-0029.

[10] B. Bazooyar, H. Gohari Darabkhani, Design, manufacture and test of a micro-turbine renewable energy combustor, Energy Convers Manag 213 (2020). https://doi.org/10.1016/j.enconman.2020.112782.

[11] G.B. Ariemma, G. Langella, P. Sabia, G. Sorrentino, M. de Joannon, R. Ragucci, Combustion stage configurations for intercooled regenerative reheat gas turbine systems, Appl Therm Eng 246 (2024). https://doi.org/10.1016/j.applthermaleng.2024.122942.

[12] H. Yilmaz, O. Cam, S. Tangoz, I. Yilmaz, Effect of different turbulence models on combustion and emission characteristics of hydrogen/air flames, Int J Hydrogen Energy 42 (2017) 25744–25755. https://doi.org/10.1016/J.IJHYDENE.2017.04.080.

[13] S. Karyeyen, Combustion characteristics of a non-premixed methane flame in a generated burner under distributed combustion conditions: A numerical study, Fuel 230 (2018) 163–171. https://doi.org/10.1016/j.fuel.2018.05.052.

[14] C. Gong, S. Zhao, W. Chen, W. Li, Y. Zhou, M. Qiu, Numerical study on the combustion process in a gas turbine combustor with different reference velocities, Advances in Aerodynamics 5 (2023). https://doi.org/10.1186/s42774-023-00154-0.

[15] M.S. Zahir, H. Hasini, N.I. Om, B.W. Riyandwita, N. Mansyur, CFD Investigation of Methane Combustion with Excess Air in Can-Type Gas Turbine Combustor, Jurnal Kejuruteraan 36 (2024) 233–248. https://doi.org/10.17576/jkukm-2024-36(1)-22.

[16] J. Chen, J. Du, Y. Liu, L. Liu, A. Li, J. Jiang, P. Sun, Numerical study of combustion flow field characteristics of industrial gas turbine under different fuel blending conditions, Appl Therm Eng 251 (2024) 123573. https://doi.org/10.1016/J.APPLTHERMALENG.2024.123573.

[17] Y. Zhao, M. Li, T. Zhou, W. Shang, Z. Ge, Experimental and numerical study on a cavity-swirler-based combustion strategy for advanced gas turbine engine, Appl Therm Eng 241 (2024) 122470. https://doi.org/10.1016/J.APPLTHERMALENG.2024.122470.

[18] H. Liu, Z. Zeng, K. Guo, Numerical analysis on hydrogen swirl combustion and flow characteristics of a micro gas turbine combustor with axial air/fuel staged technology,

Power System Technology
ISSN:1000-3673
Received: 06-06-2024 Revised: 15-07-2024 Accepted: 28-08-2024

Appl Therm Eng 219 (2023) 119460. https://doi.org/10.1016/J.APPLTHERMALENG.2022.119460.

[19] ANSYS FLUENT 12.0 Theory Guide - 1.2 Continuity and Momentum Equations, (n.d.). https://www.afs.enea.it/project/neptunius/docs/fluent/html/th/node11.htm (accessed February 22, 2024).

[20] Athanasios Alexakis, CFD Modelling of Stirling Engines with Complex Design Topologies , University of Northumbria at Newcastle, 2013.

[21] C. Chi, J. Mou, M. Lin, G. Hong, CFD simulation and investigation on the operating mechanism of a beta-type free piston Stirling engine, Appl Therm Eng 166 (2020) 114751. https://doi.org/10.1016/j.applthermaleng.2019.114751.

[22] ANSYS FLUENT 12.0 Theory Guide - 4.4.1 Standard - Model, (n.d.). https://www.afs.enea.it/project/neptunius/docs/fluent/html/th/node58.htm (accessed February 22, 2024).

[23] ANSYS FLUENT 12.0 Theory Guide - 5.2.1 Heat Transfer Theory, (n.d.). https://www.afs.enea.it/project/neptunius/docs/fluent/html/th/node107.htm#eq-energy-E (accessed February 22, 2024).

[24] ANSYS FLUENT 12.0 Theory Guide - 8. Non-Premixed Combustion, (n.d.). https://www.afs.enea.it/project/neptunius/docs/fluent/html/th/node142.htm (accessed May 12, 2024).